Tellus (1986), *38B*, 223–235

Aerosol measurements at the South Pole

By BARRY A. BODHAINE, JOHN J. DELUISI, JOYCE M. HARRIS, *Geophysical Monitoring for Climatic Change, NOAA Air Resources Laboratory, 325 Broadway, Boulder, Colo. 80303, USA* and PAMELA HOUMERE and SENE BAUMAN, *4 meV PIXE Laboratory, Florida State University, Tallahassee, Fla. 32306 USA*

(Manuscript received October 3, 1985; in final form January 27, 1986)

ABSTRACT

The Geophysical Monitoring for Climatic Change (GMCC) program of the National Oceanic and Atmospheric Administration (NOAA) operates an atmospheric monitoring observatory at Amundsen-Scott Station, South Pole. Long-term measurements of carbon dioxide, ozone, aerosols, and other background pollutants are obtained to understand their possible effects on the earth's climate. The aerosol measurement program consists of the continuous measurement of condensation nuclei (CN) concentration and aerosol scattering extinction coefficient (σ_{sp}).

During 1982, Nuclepore-filter aerosol samples were taken for subsequent analysis by the proton-induced X-ray emission (PIXE) technique with 8-h time resolution. A time series of sodium, chlorine, and sulfur concentrations shows that the sulfur and CN records are similar and that the sodium, chlorine, and σ_{sp} records are similar. Large episodes of sodium are measured at the ground in the austral winter and are apparently caused by large-scale transport from coastal regions and vertical transport to the surface during times of surface warming and weakening of the surface temperature inversion. These episodes are characterized by increases in sodium concentration, Cl/Na ratio, σ_{sp}, and particle size, and decreases in non-sea-salt sulfur concentration, suggesting a decrease in atmospheric acidity and a displacement of sulfuric acid aerosol. An analysis of back trajectories suggests transport times of several days from the Antarctic coast.

A nearly continuous record of South Pole CN measurements from 1974 to the present, and σ_{sp} measurements from 1979 to the present, has now been accumulated. The CN data show an annual cycle with a maximum exceeding 100 cm^{-3} in the austral summer and a minimum of about 10 cm^{-3} in the winter. The σ_{sp} data show an annual cycle markedly different from that of CN with a maximum in late winter, a secondary maximum in summer, and a minimum in May. Angstrom exponents calculated from the multiwavelength σ_{sp} data show a strong annual cycle suggesting larger particles in the winter than in the summer.

1. Introduction

The Geophysical Monitoring for Climatic Change (GMCC) program of the National Oceanic and Atmospheric Administration (NOAA) operates 4 observatories located at Barrow, Alaska; Mauna Loa, Hawaii; American Samoa; and South Pole. The mission of the GMCC program is to measure the atmospheric concentrations of climatically important gases and aerosols over a long term and to investigate potential climatic effects of both natural and anthropogenic emissions. The Amundsen-Scott Station, located at the Geographic South Pole and operated by the National Science Foundation, was established for the International Geophysical Year in 1956. The first GMCC measurements at the South Pole were made at the Aurora tower in 1974, and from a temporary structure built under the snow in 1975 and 1976. In January 1977, the GMCC program moved into the newly constructed Clean Air Facility (CAF). Fig. 1 shows the location of the CAF, upwind of the remainder of the station including

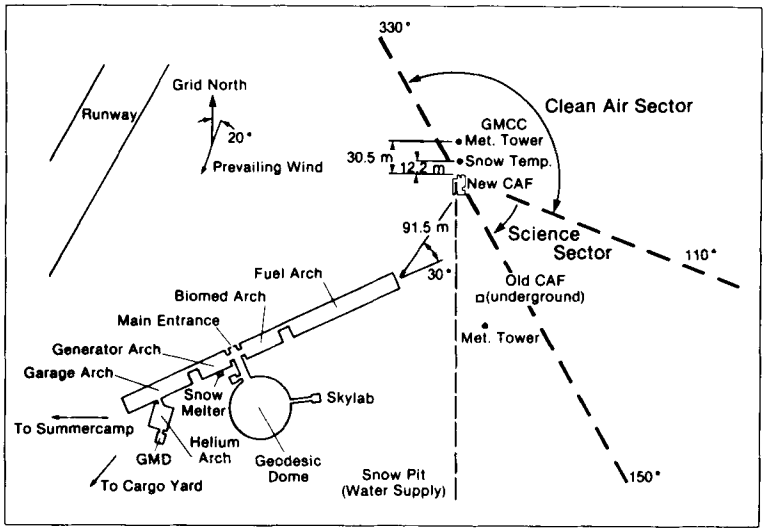

Fig. 1. Amundsen-Scott Station, showing the CAF relative to the rest of the camp.

the dome that houses the living quarters and the arches that house the power plant.

A wind rose showing the frequency of winds as a function of direction for 1977–1983 at the CAF is presented in Fig. 2. Winds are from the clean-air sector (Fig. 1) more than 98% of the time, a result of the persistent katabatic winds from the polar plateau. Data taken at the CAF are adequately screened on the basis of wind direction to remove possible effects of local pollution produced at the camp.

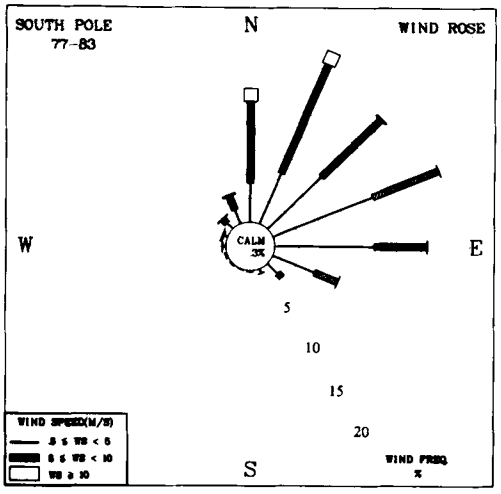

Fig. 2. Wind rose showing the frequency of winds as a function of direction for 1977–1983 at the South Pole.

The GMCC four-wavelength nephelometer was installed at the South Pole in January 1979. The first year of aerosol scattering extinction (σ_{sp}) data, presented by Bodhaine and Bortniak (1981) and Parungo et al. (1981), showed an annual cycle strikingly different from the CN record, being dominated by sea-salt events in the austral winter. Because of the 3.8 h time constant of the nephelometer, individual sea-salt events were easily identified and could be correlated with the local meteorology. An aerosol chemistry experiment was planned for the year 1982 which would allow for an aerosol elemental analysis with 8 h time resolution, sufficient for a detailed comparison with local and large-scale meteorology.

The purpose of this paper is to present the results of the 1982 aerosol chemistry experiment, give a brief review of aerosol work at the South Pole, update the GMCC South Pole aerosol data set through 1984, and discuss some possible meteorological situations responsible for the transport of sea salt to the South Pole. Large-scale isentropic back trajectories were calculated to identify preferred transport routes and source regions.

Apparently the first published measurements of atmospheric particles at the South Pole were

by Duce et al. (1971), Duce (1972), Duce et al. (1973), Zoller et al. (1974), and Duce et al. (1975). They presented elemental concentrations for filter samples taken in the 1970–1971 austral summer. The continuation of this work by Maenhaut and Zoller (1977), Maenhaut et al. (1979), Cunningham et al. (1979), and Cunningham and Zoller (1981) produced an excellent data set describing the South Pole aerosol chemistry. The chemistry of individual particles was studied by Fischer et al. (1969) and Parungo et al. (1979, 1981).

Condensation nucleus (CN) concentration at the South Pole was first studied by Hogan (1975), and transport processes were discussed by Hogan and Barnard (1978), Hogan (1979), and Hogan et al. (1982). Vertical CN profiles were given by Hogan (1979), and size distribution measurements were performed by Hogan et al. (1979). The complete CN record was presented by Murphy and Bodhaine (1980), and the record was updated through 1981 by Bodhaine (1983).

The GMCC aerosol monitoring program includes the continuous measurement of CN concentration and σ_{sp} at the wavelengths 450, 550, 700, and 850 nm. Because these four wavelengths encompass the visible spectrum, the σ_{sp} measurements are more representative than the CN concentration measurements of aerosols that may interact with the radiation field and influence climate. The σ_{sp} measurements are most sensitive to particles having diameters in the 0.1- to 1.0 μm diameter range (the accumulation mode) whereas CN concentrations tend to be dominated by particles smaller than 0.1 μm diameter (the Aitken mode). Since particles in the 0.1- to 1.0 μm range tend to dominate the total background atmospheric aerosol mass, σ_{sp} is often representative of aerosol mass. The CN measurements provide a good indication of any local pollution events that could interfere with the routine monitoring program.

2. Experimental

During 1982, aerosol samples for subsequent proton induced X-ray emission (PIXE) analysis (Johansson et al., 1975) were taken using a circular streaker sampler. This sampler uses an 8 cm diameter Nuclepore filter (0.3 μm pore diameter) mounted on a frame that rotates at one revolution per month. The filter slides along a 2 mm × 4 mm rectangular sucking orifice operating at about 1 litre/min, thus producing a streak of sampled aerosol that can then be analyzed for elemental concentration as a time series by the PIXE method. This analysis produced data with 8 h time resolution for the elements sodium, chlorine, and sulfur. All other elements were below the detection limits of the method for these particular samples because of the extremely small aerosol concentrations found at the South Pole. Blanks were also analyzed on unused portions of the streaker filters. Blank values were about the same as the minimum detection limits (slightly higher for chlorine), and were subtracted from the data. Whenever the blank value exceeded a particular data value, the value was set to zero. Aerosol loading on the Nuclepore filter was so light at the South Pole that pore clogging was never a problem.

Condensation nucleus concentration is measured continuously using a General Electric automatic CN counter (Skala, 1963) with modifications to the electronics suggested by Norman Ahlquist of the University of Washington. This instrument produces an expansion in a cloud chamber that causes aerosol particles in a humidified air sample to grow into water droplets at a supersaturation of about 300%. The intensity of the resulting cloud is then detected by optical means. A Pollak photoelectric nucleus counter (Metnieks and Pollak, 1959) is used as an on-site standard to obtain daily calibration points for the automatic CN counter (Bodhaine and Murphy, 1980). The Pollak counter is also an expansion instrument using optical means to detect cloud droplets in a cloud chamber. A review of CN counters was given by Miller and Bodhaine (1982).

The aerosol scattering extinction coefficient is measured continuously at the 450, 550, 700, and 850 nm wavelengths using a specially constructed four-wavelength nephelometer similar in design to that described by Ahlquist and Charlson (1969). By using a real-time subtraction to eliminate the molecular scattering of air, this instrument is capable of measuring σ_{sp} values as low as about 10^{-7} m^{-1}, approximately 1% of Rayleigh scattering by air molecules. The

nephelometer is calibrated by filling it with carbon dioxide gas (Bodhaine, 1979).

Three values of Angstrom exponent may be calculated from the four successive σ_{sp} values according to the formula $\alpha = -\Delta \log \sigma_{sp}/\Delta \log \lambda$, where α is the Angstrom exponent and λ is the wavelength. The interpretation of α for the multi-wavelength nephelometer has been discussed by Thielke et al. (1972). Assuming a power law relationship, $dN/dr \propto r^{-\nu}$, for an aerosol size distribution, then theoretically $\sigma_{sp} \propto \lambda^{-\alpha}$, and $\nu = \alpha + 3$, where dN is the concentration in the radius interval dr, r is the aerosol radius, and ν is the slope of the aerosol size distribution (Van de Hulst, 1957). In general, a large α implies an aerosol size distribution biased toward small particles, and a small α implies a bias toward large particles. Although a power law aerosol size distribution is not a reasonable assumption over the entire range of aerosol sizes and the above result cannot be strictly applied, the three-segment approximation for the Angstrom exponent does show significant variations and can be interpreted qualitatively in terms of variations in the aerosol size distribution.

The air sampling intakes used at GMCC observatories were described by Komhyr (1983). At the South Pale CAF, an anodized aluminum sampling stack with an inlet height of 13 m supplies air through isokinetic sampling nozzles to the instruments inside the building. The CN counters each draw about 6 l min^{-1} through 1 m of 0.6 cm diameter tubing. The nephelometer draws about 30 l min^{-1} through 3 m of 3.2 cm diameter tubing. The sampled air approaches 0% relative humidity because it is warmed from the outside temperatures of between -20 and -80°C to an inside temperature of about 20°C before it reaches the instruments. Aerosol losses in the sampling tubes, calculated using the methods outlined by Dennis (1976), are negligible in the size range of interest.

3. Results

3.1. 1982 experiment

The time series of 8 h mean sulfur and sodium concentrations plotted along with daily mean CN concentration and σ_{sp} (550 nm) for the year 1982 is shown in Fig. 3. The annual trends of sulfur

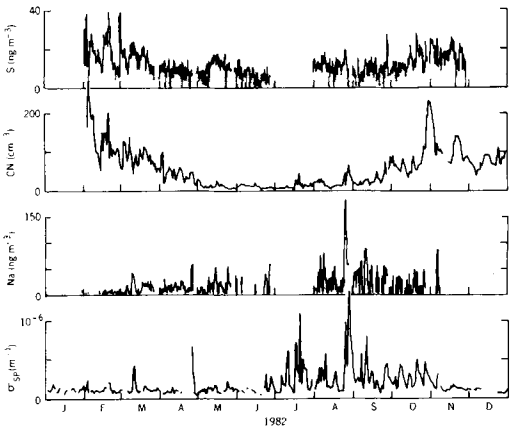

Fig. 3. Daily geometric means of σ_{sp} (550 nm), 8 h means of sodium concentration, daily geometric means of CN concentration, and 8 h means of sulfur concentration for 1982 at the South Pole.

and CN concentration are similar, as are those of sodium and σ_{sp}, implying that sulfur is contained primarily in the small-particle size range and sodium is in the large-particle size range. Furthermore, when comparing the sodium and σ_{sp} records, the individual events coincide well. Unfortunately, the large event on August 29 is missing from the sodium and sulfur data because the streaker sampler did not operate during the last 3 days of the month.

Fig. 4 shows the sodium and σ_{sp} (550 nm) data for August–September, 1982. Here the σ_{sp} data are plotted as 8 h means to match the times of the sodium data. In general, the times of occurrence and relative strengths of all the events are

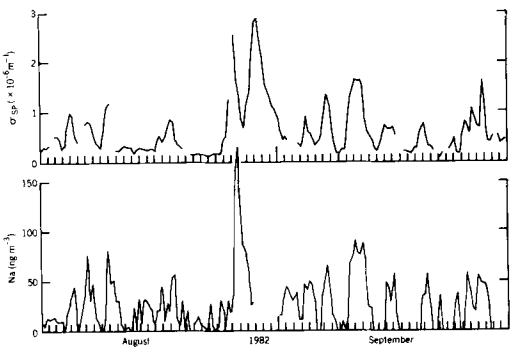

Fig. 4. Eight-hour means of sodium concentration (lower) and σ_{sp} (upper) for August–September 1982 at the South Pole.

in good agreement. A correlation coefficient of 0.75 ± 0.07 at a 95% confidence level was found for the sodium and σ_{sp} data during August–September. To study the causes of these events more closely, South Pole radiosonde data for the time period 20 August–17 September 1982 were used to produce the vertical time cross section of temperature shown in Fig. 5. Superposed on this time section are the σ_{sp} (550 nm) data for the same time period. Clearly the large aerosol events recorded at the surface are associated with periods of warming in the 650–550 mb layer, warming at the surface, and a decrease in the strength of the surface temperature inversion. Fig. 6 shows 270 K isentropic trajectories (Harris and Bodhaine, 1983) calculated backward from the South Pole on 9 September 1982, before the large September event, and on 11 September 1982, at the peak of the event. The trajectory at 1200 GMT on 9 September and those at 0000 and 1200 GMT on 11 September show rapid transport of air from the coast to the Pole in 1–2 days. Trajectories before (such as 0000 GMT on 9 September in Fig. 6) and after the event are uncertain, meander around, and move slowly whereas trajectories during the event are similar to those shown for 11 September. A map of the 500 mb height field over the Antarctic continent on 9 September 1982 (Fig. 7) shows a deep low-pressure system over the Ross Sea that is responsible for this rapid transport of air to the Pole. A time series of these charts shows the low reaching its deepest point on 9 September and then beginning to dissipate on 11 September.

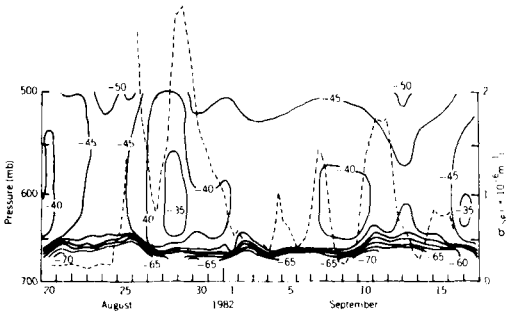

Fig. 5. Vertical time cross section of temperature (solid) and daily geometric means of σ_{sp} (550 nm) (dashed) for 20 August–17 September 1982 at the South Pole.

Fig. 8 shows a scatter diagram of chlorine vs. sodium concentrations for August–September 1982, where the straight line shows the sea-water Cl/Na ratio of 1.79 (a data value of zero was plotted on the axis). Three regions are apparent on this diagram. At the highest concentrations, the data points cluster near the sea-water ratio; at intermediate concentrations, the points tend to fall below the line; and at low concentrations (near the detection limit of about 10 ng m^{-3}), the points show large random scatter. Fig. 9 shows the time series of sodium, chlorine, sulfur, sea-salt sulfur, and non-sea-salt sulfur concentrations, along with Cl/Na ratios, for August–September 1982. Sea-salt sulfur concentration was calculated using the standard sea-water S/Na ratio of 0.0837. The remaining sulfur in the sample was considered to be non-sea-salt sulfur. Chlorine and sodium concentrations for the large aerosol peak

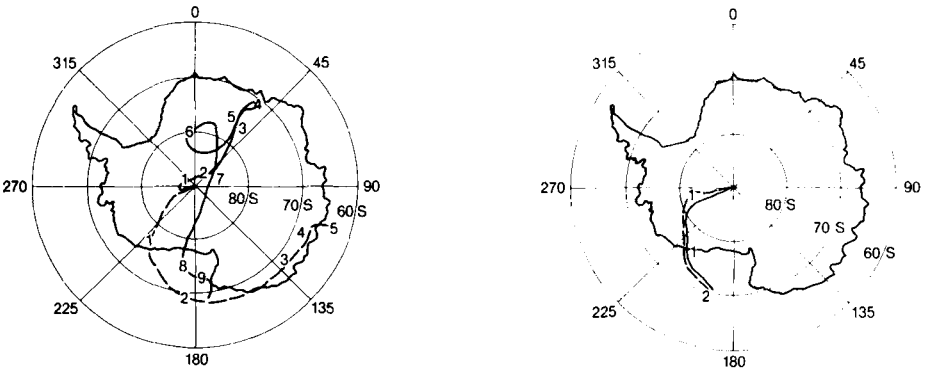

Fig. 6. Isentropic trajectories calculated backward from the South Pole at 0000 GMT (solid) and 1200 GMT (dashed) on 9 September (left) and 11 September (right) 1982 at the 270-K potential temperature level.

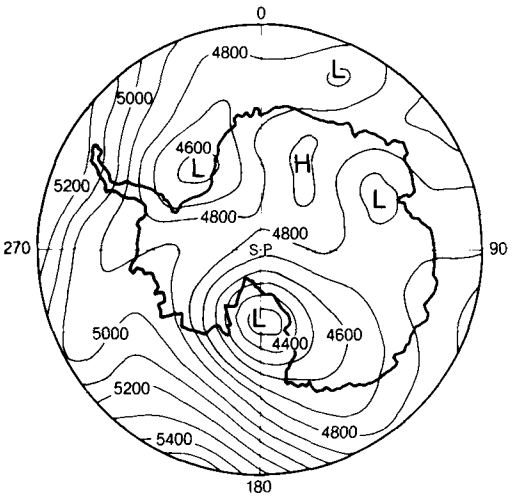

Fig. 7. Height contours (m) of the 500-mb surface over Antarctica at 1200 GMT on 9 September 1982.

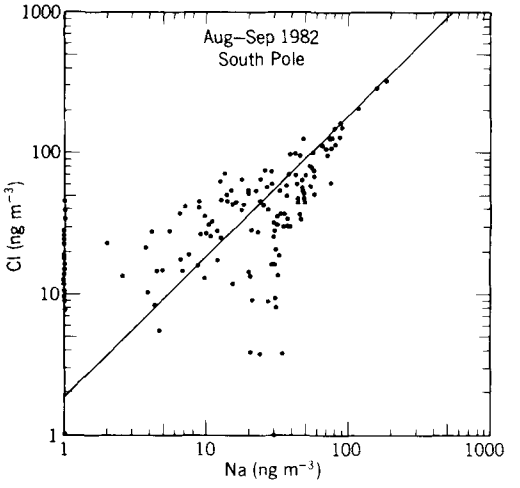

Fig. 8. Scatter plot of chlorine versus sodium concentration for each 8 h aerosol sample during August–September 1982. The diagonal line shows the standard sea-water Cl/Na ratio of 1.79.

of 26 August were 328 ng m^{-3} and 185 ng m^{-3} respectively, giving Cl/Na = 1.77, which is close to the sea water value of 1.79. The sulfur concentration during this peak was 19.2 ng m^{-3}, or 3.7 ng m^{-3} non-sea-salt sulfur. The time series in Fig. 9 during this event shows that Cl/Na values generally increased from < 1 to about 1.77 during the event and then back to values that

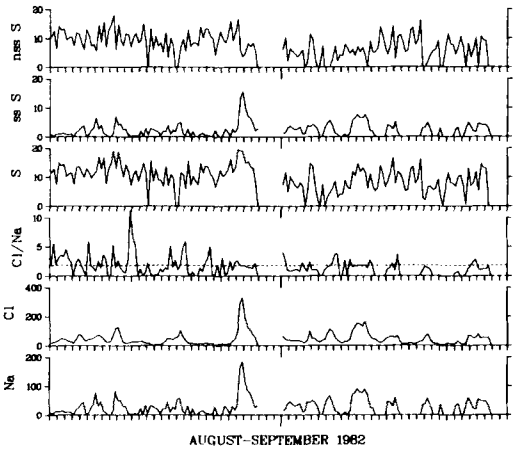

Fig. 9. 8 h mean concentrations (from top to bottom) of non-sea-salt sulfur, sea-salt sulfur, total sulfur, Cl/Na ratio, chlorine, and sodium for August–September 1982 at the South Pole. All concentrations are given in ng·m^{-3} except Cl/Na which is dimensionless. The dashed line shows the sea-water Cl/Na ratio of 1.79.

were < 1. The sulfur concentrations increased from about 10 ng m^{-3} to 19.2 ng m^{-3} and then decreased back to about 10 ng m^{-3}. Non-sea-salt sulfur decreased from about 10 ng m^{-3} to 3.7 ng m^{-3} and then increased back to about 10 ng m^{-3}. These results are consistent with a background acidic (sulfate) aerosol with depleted chlorine, which is often displaced by a sea-salt aerosol event that shows the correct sea-water Cl/Na ratio and a decrease in the non-sea-salt sulfur.

3.2. 1979 experiment

The largest σ_{sp} event recorded at the South Pole occurred on 1 August 1979 (see Fig. 20). The largest hourly mean value on that day was σ_{sp} (550 nm) = 1.54×10^{-5} m^{-1}. This value is comparable with the average value measured in the marine boundary layer at Samoa (Bodhaine, 1983). A vertical time cross section of temperature for 26 July–6 August 1979 with this σ_{sp} event superposed is shown in Fig. 10. Again we see a warming at about 600 mb, a surface warming, and a weakening of the surface inversion. This particular event was identified chemically as sea salt by Parungo et al. (1981) and discussed in more detail by Bodhaine and Bortniak (1981). Back trajectories meandered on the continent before the event at 0000 GMT on 1 August 1979

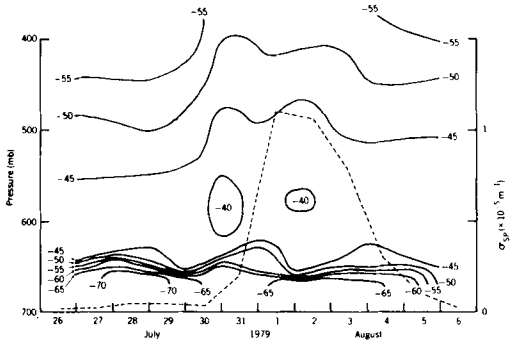

Fig. 10. Vertical time cross section of temperature (solid) and daily geometric means of σ_{sp} (550 nm) (dashed) for 26 July–6 August 1979 at the South Pole.

as shown in Fig. 11 (left). However, at 1200 GMT on the same day, transport was rapid and direct from coastal regions. Throughout the event, trajectories were similar to those shown for 0000 and 1200 GMT on 4 August 1979 in Fig. 11 (right). After the event, trajectories showed slow and meandering transport.

3.3. *Long-term data set*

Condensation nucleus concentration (solid) and σ_{sp} at 550 nm (dashed) as a function of wind direction for 1981 are shown in Fig. 12. As expected, CN concentration is significantly higher when winds are not from the clean-air sector. Local pollution from the camp shows up clearly in the CN concentration data and, to a lesser extent, in the σ_{sp} data. In general, however, as seen in the wind frequency data of Fig. 2, the wind rarely comes from outside the clean-air sector, and therefore the local sources rarely influence the data. Often during the winter the winds are quite constant for months at a time from the clean air sector.

Monthly geometric means of CN, σ_{sp}, and Alpha data, calculated from hourly data for the entire record, are presented in Fig. 13. For clarity, only one channel of the σ_{sp} data (550 nm) is shown. The straight dashed lines are least squares straight lines fit to the common logarithms of the CN and σ_{sp} data, and linearly to the Alpha data, to represent possible long-term trends. A listing of the monthly means is given in Table 1, and results of the linear regression are given in Table 2. Grand geometric means of the entire data set are given in Table 3. Note that the means, standard deviations, and standard errors about the regression lines are given for the common logarithms of the data points for CN and σ_{sp}.

The long-term record of CN (Fig. 13, lower) shows an extremely regular annual cycle with a minimum of about 10 cm^{-3} in the austral winter and a maximum exceeding 100 cm^{-3} in summer. This annual cycle is well known and has been discussed by Hogan et al. (1982). The long-term record of σ_{sp} (Fig. 13, middle) shows a more complicated annual cycle with largest values during late winter. The Angstrom exponent record (Fig. 13, upper) also shows an annual cycle with a tendency toward smaller sized particles during the austral summer and larger particles in the late

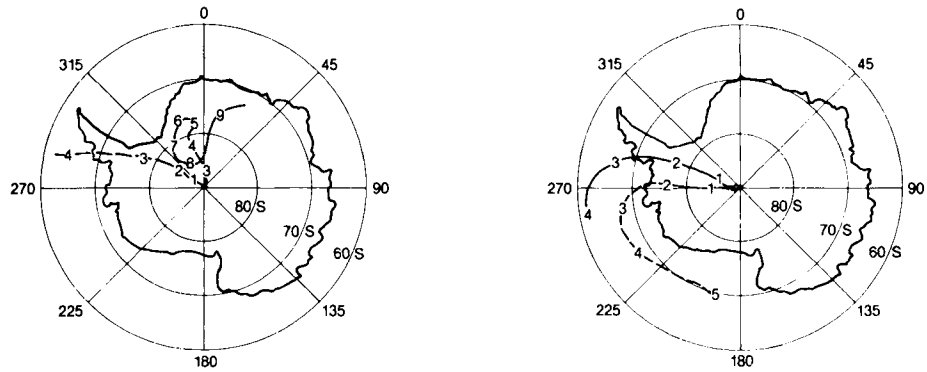

Fig. 11. Isentropic trajectories calculated backward from the South Pole at 0000 GMT (solid) and 1200 GMT (dashed) on 1 August (left) and 4 August (right) 1979 at the 275-K potential temperature level.

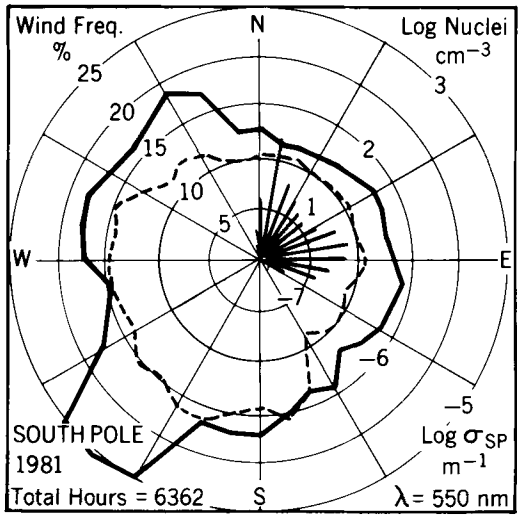

Fig. 12. 36-point wind rose showing CN concentration (solid) and σ_{sp} at 550 nm (dashed) as a function of wind direction for the South Pole in 1981. Wind direction frequency for the data set is shown by the bars in the center.

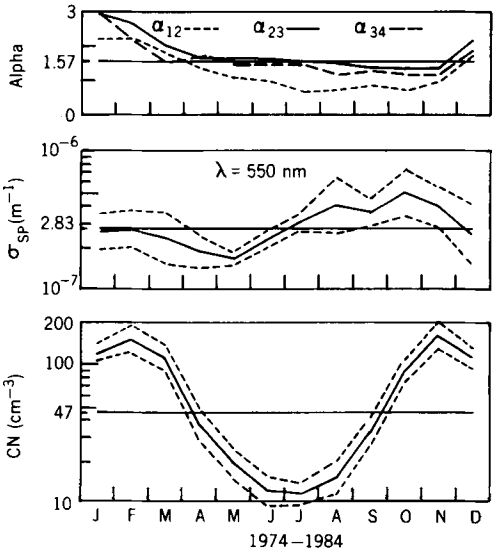

Fig. 14. Geometric means by month of South Pole CN concentration (lower), σ_{sp} at 550 nm (middle), and Angstrom exponent (upper). Dashed lines on the CN and σ_{sp} plots show one standard deviation.

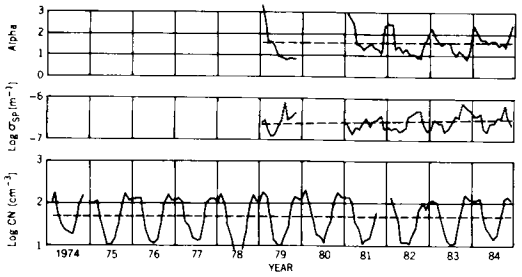

Fig. 13. South Pole monthly geometric means of CN concentration (lower), σ_{sp} at 550 nm (middle), and mean Angstrom exponent (upper). A listing of the data is given in Table 1, and details of the trend lines (dashed) are given in Table 2.

austral winter. In general, a large σ_{sp} episode will most likely be produced by an accumulation mode (or larger) aerosol because an Aitken mode aerosol is a low efficiency scatterer. A wind-blown soil-dust aerosol or a sea-salt aerosol will give high σ_{sp} and small Angstrom exponents.

The trend for the CN data of about -0.7% year^{-1} (Table 2) is not statistically significant. The increasing trends for σ_{sp} and Angstrom exponent are not statistically significant and have varied considerably as more years have been added to the data set, clearly because of the short record.

To study the annual cycles in σ_{sp} and CN concentration, geometric means by month for the entire data record were calculated and are presented in Fig. 14. Long-term trends were not removed from the data before monthly means were calculated because they are not statistically significant. The annual cycle in CN concentration is obvious, showing a maximum in the summer and a minimum in winter. The geometric standard deviations (dashed lines in Fig. 14, lower) suggest a small year-to-year variability that is relatively constant from month to month. Hogan et al. (1982) suggested that the low winter values occur because of reduced vertical exchange across the strong surface temperature inversion. Ito (1985) suggested that the CN concentration increases with the cosine of the solar zenith angle, and, therefore, a change in the rate of gas-to-particle conversion in the sub-Antarctic regions along with transport to the South Pole could be responsible for the annual cycle.

The annual cycle in σ_{sp} (Fig. 14, middle) shows large values in the late austral winter that are most likely caused by transport of sea salt from

Table 1. *South Pole monthly geometric means of CN concentration (cm^{-3}) and σ_{sp} (10^{-7} m^{-1}) at 450, 550, 700, and 850 nm*

	JAN	FEB	MAR	APR	MAY	JUN	JUL	AUG	SEP	OCT	NOV	DEC
1974 CN	-	97	178	52	31	23	20	18	41	95	153	-
1975 CN	99	106	113	41	21	10	11	15	31	79	173	114
1976 CN	125	132	125	62	21	13	11	14	32	98	166	115
1977 CN	123	136	105	37	28	15	13	13	32	107	133	132
1978 CN	103	168	91	31	18	7	8	7	21	77	152	113
1979 CN	111	185	143	50	14	11	10	17	28	90	144	118
$\sigma_{sp}(450)$	4.65	4.86	2.45	1.38	1.45	2.07	2.94	8.28	3.23	3.76	5.10	-
$\sigma_{sp}(550)$	2.72	3.14	1.95	1.23	1.41	2.16	2.93	7.94	3.14	3.74	4.66	-
$\sigma_{sp}(700)$	1.22	1.74	1.36	0.80	0.98	1.59	2.29	6.25	2.48	2.91	3.81	-
$\sigma_{sp}(850)$	0.55	0.92	0.89	0.49	0.64	1.15	1.72	4.97	1.84	2.22	3.08	-
1980 CN	134	211	98	46	18	17	11	22	38	103	183	136
1981 CN	139	144	98	35	25	11	15	16	29	62	-	-
$\sigma_{sp}(450)$	4.03	3.62	2.37	3.26	2.52	3.09	3.78	2.65	3.78	4.03	4.59	2.93
$\sigma_{sp}(550)$	2.78	2.08	1.34	2.20	1.84	2.49	3.43	2.08	2.97	3.23	3.97	1.85
$\sigma_{sp}(700)$	1.17	0.99	0.71	1.54	1.26	1.72	2.07	1.27	2.05	2.18	2.88	1.00
$\sigma_{sp}(850)$	0.57	0.62	0.47	1.23	1.02	1.41	1.50	0.96	1.58	1.78	2.36	0.65
1982 CN	-	140	80	40	12	12	11	18	26	71	105	70
$\sigma_{sp}(450)$	3.09	2.86	2.79	2.27	2.20	2.75	4.45	5.39	5.77	5.35	3.26	2.31
$\sigma_{sp}(550)$	2.08	1.82	2.10	1.70	1.82	2.09	3.82	4.49	5.17	4.86	2.47	1.61
$\sigma_{sp}(700)$	1.05	0.85	1.35	1.22	1.31	1.45	2.77	3.21	3.76	3.58	1.64	0.94
$\sigma_{sp}(850)$	0.64	0.57	1.20	0.92	1.07	1.18	2.27	2.81	3.32	3.08	1.25	0.71
1983 CN	103	122	100	43	24	14	10	12	32	86	158	119
$\sigma_{sp}(450)$	3.02	4.75	3.60	3.46	2.27	2.70	3.36	4.64	4.35	9.28	7.25	6.42
$\sigma_{sp}(550)$	1.85	3.16	2.63	2.60	1.55	1.95	2.69	3.98	3.39	7.91	6.26	5.14
$\sigma_{sp}(700)$	1.00	1.85	1.69	1.82	0.95	1.24	1.89	2.95	2.36	5.99	4.99	3.34
$\sigma_{sp}(850)$	0.70	1.39	1.23	1.35	0.78	0.96	1.59	2.48	1.94	4.89	4.33	2.81
1984 CN	117	111	126	43	25	18	14	18	43	116	138	111
$\sigma_{sp}(450)$	6.34	6.00	6.69	2.40	1.89	3.36	3.38	4.27	4.75	9.00	4.82	3.39
$\sigma_{sp}(550)$	4.09	3.89	4.55	1.84	1.62	2.77	2.81	3.65	3.69	7.27	3.49	2.37
$\sigma_{sp}(700)$	2.30	2.24	2.73	1.12	0.98	1.75	1.80	2.38	2.59	4.99	2.02	1.39
$\sigma_{sp}(850)$	1.39	1.63	2.18	0.76	0.68	1.14	1.14	1.70	1.74	3.73	1.43	0.75

coastal regions (Bodhaine and Bortniak, 1981; Parungo et al., 1981; Bodhaine, 1983). The year-to-year variability (dashed lines) is small compared with the annual change. The largest variability in σ_{sp} appears in August because the sea-salt events are episodic and highly variable from year to year.

The annual cycle in Angstrom exponent (Fig. 14, upper) is interesting because it shows a decrease from January to October, implying an increase in the relative numbers of large particles during this period. This is consistent with the appearance of higher values of σ_{sp} caused by the transport of sea salt. The maximum Angstrom exponents occur in the austral summer, coincident with maximum CN, implying an absence of larger particles such as sea salt. The lowest values of Angstrom exponent, occurring during late austral winter and early spring, are caused by the influx of sea-salt particles. These data are in good agreement with those of Cunningham and Zoller (1981), who describe the annual trends of sulfate, crustal elements, and sea salt. The CN data presented here follow the sulfate trend closely. The σ_{sp} trend shows a combination of the sulfate and sea salt trends, the relative maximum in summer being caused by increased sulfate and reduced sea salt (which would otherwise dominate σ_{sp}).

To study possible diurnal effects in the South Pole aerosol, hourly geometric means by month were calculated for CN concentration and σ_{sp}.

Table 2. *Geometric least-squares trend analyses of CN and σ_{sp} (550) data, and linear least-squares analysis of Alpha data presented in Fig. 13*

	Slope	Intercept	S.E.	Trend (year)$^{-1}$
CN	-2.66×10^{-4}	1.69	0.429	−0.73%
σ_{sp} (550 nm)	2.09×10^{-3}	−6.76	0.189	5.9%
α	2.50×10^{-4}	1.55	0.611	0.19%

The scale of the abscissa is such that January 1974 = 1 and December 1984 = 132.

S.E. = standard error about the regression line.

Table 3. *Grand geometric means and standard deviations using common logarithms for the CN and σ_{sp} data given in Table 1*

	Geometric mean	Mean and standard deviation of logarithms of data points
CN	47 cm^{-3}	1.6705 ± 0.4427
σ_{sp} (450)	3.65×10^{-7} m^{-1}	−6.4378 ± 0.1809
σ_{sp} (550)	2.83×10^{-7} m^{-1}	−6.5488 ± 0.1922
σ_{sp} (700)	1.82×10^{-7} m^{-1}	−6.7392 ± 0.2254
σ_{sp} (850)	1.33×10^{-7} m^{-1}	−6.8762 ± 0.2611
α_{12}	1.28	
α_{23}	1.82	
α_{34}	1.63	

Angstrom exponents were calculated from the grand geometric means of σ_{sp}.

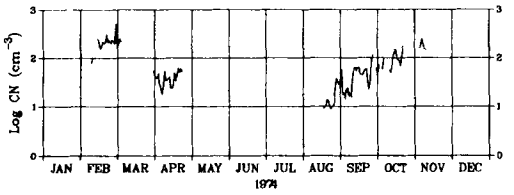

Fig. 15. South Pole daily geometric means of CN concentration for 1974.

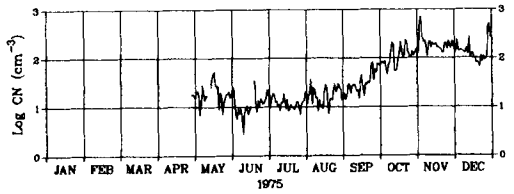

Fig. 16. Same as Fig. 15, but for 1975.

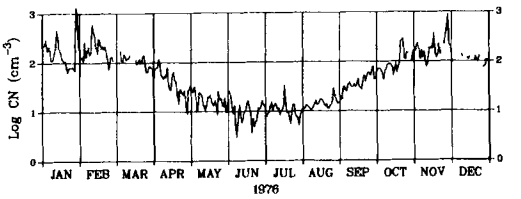

Fig. 17. Same as Fig. 15, but for 1976.

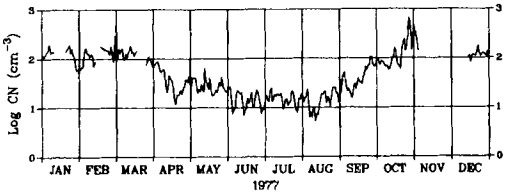

Fig. 18. Same as Fig. 15, but for 1977.

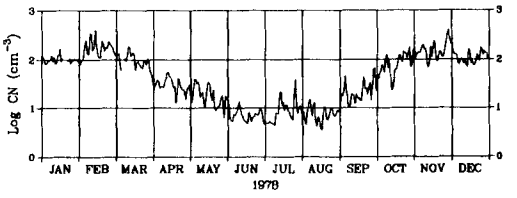

Fig. 19. Same as Fig. 15, but for 1978.

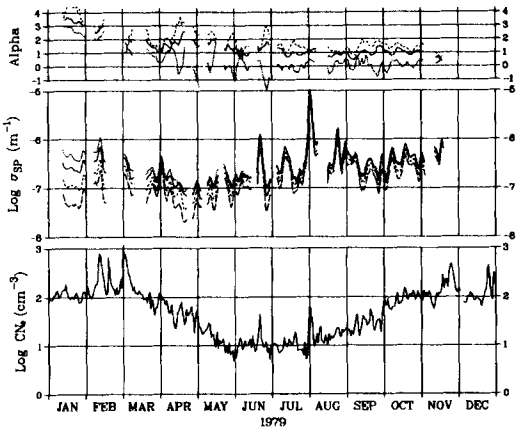

Fig. 20. South Pole daily geometric means of CN concentration (lower), σ_{sp} (middle), and Angstrom exponent (top), for 1979. σ_{sp} data are shown for 450 nm (dotted), 550 nm (solid), 700 nm (dashed), and 850 nm (long dashed). Angstrom exponent data are shown for α_{12} (dotted), α_{23} (solid), and α_{34} (dashed).

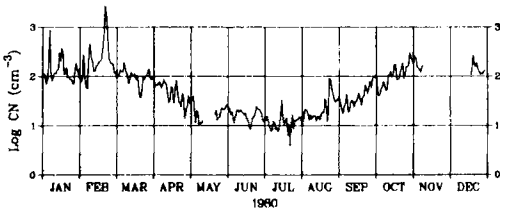

Fig. 21. Same as Fig. 15, but for 1980.

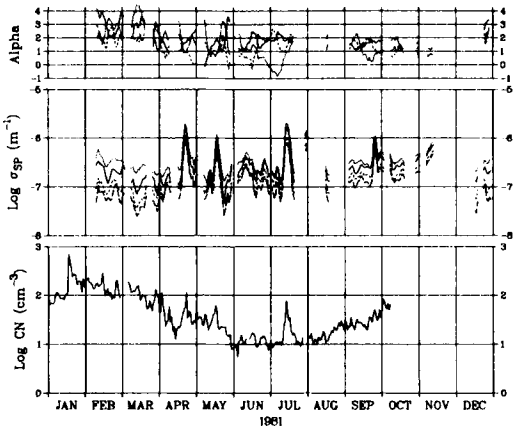

Fig. 22. Same as Fig. 20, but for 1981.

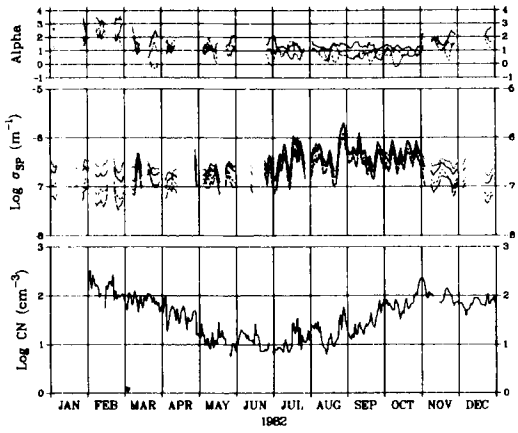

Fig. 23. Same as Fig. 20, but for 1982.

No significant diurnal cycle was found in any of the data. Because the South Pole is dark for about half the year, any diurnal effects must occur at lower latitudes and then be reflected in the South Pole data as a result of transport processes. Since the fastest transport to the Pole is on the order of several days, possible diurnal effects are averaged out.

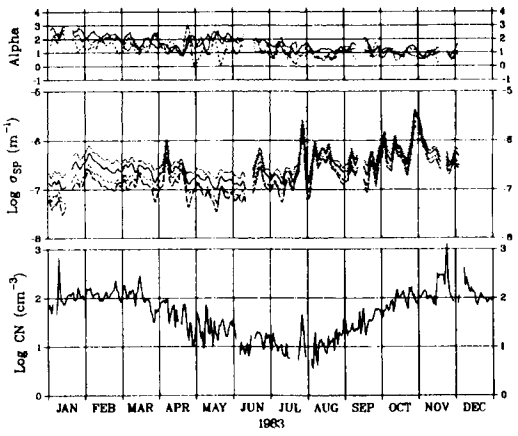

Fig. 24. Same as Fig. 20, but for 1983.

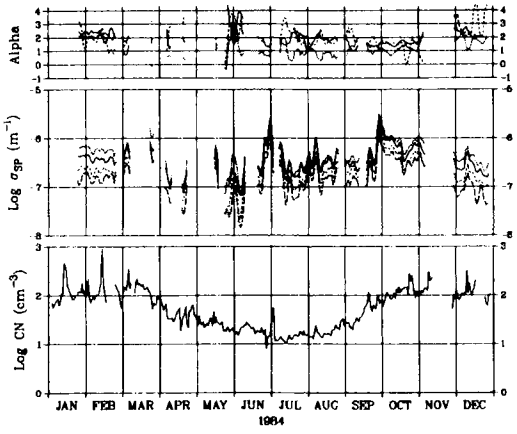

Fig. 25. Same as Fig. 20, but for 1984.

The complete data set for 1974–1984 is presented in Figs. 15–25. For the years 1974–1978 and 1980, daily geometric means are plotted for CN concentration. For 1979 and 1981–1984, daily geometric means are plotted for CN concentration (lower); σ_{sp} at 450, 550, 700, and 850 nm (middle); and Angstrom exponent (upper). All years show the characteristic annual cycle in CN concentration. The σ_{sp} data clearly show the large sea-salt events during July–October. Generally, the austral winter season is marked by a series of events, or pulses, about 2 weeks apart, in which the aerosol appears at the surface at the Pole. These events are most likely

caused by the motion of low-pressure storm systems near Antarctica that establish rapid transport paths from coastal regions to the Pole.

4. Conclusions

Surface-based aerosol measurements at the South Pole clearly show an annual cycle in CN concentration that coincides with that of sulfur and an annual cycle in σ_{sp} that coincides with that of sodium. This suggests that sulfur is contained primarily in the small-particle size range, and sodium, or sea salt, is contained primarily in the large-particle size range. Large-scale meteorological analyses and large-scale back trajectories have shown that rapid transport paths can exist from the coast of Antarctica to the interior, during which large amounts of sea-salt aerosol are transported in the troposphere to the South Pole in about 2 days. These injections of materials into the Antarctic troposphere contribute to a general build-up throughout the winter.

Since aerosol concentrations above the boundary layer can be much larger than those at the surface, the aerosol must be transported through the persistent surface temperature inversion to be detected at the surface. This vertical transport is continuously occurring to some degree; however, periods of weakening of the surface inversion could provide enhanced vertical transport to the surface. Although continuous surface measurements are the only reasonable method for obtaining a long-term record, short-term aircraft experiments such as those by Hogan (1979) or balloon experiments such as those by Hofmann and Rosen (1985) are needed for a more complete understanding of the vertical and horizontal extents of the aerosol. A surface-based tropospheric lidar operated regularly at the South Pole could provide important information. Unfortunately, these types of experiments are difficult during the austral winter.

Large sea-salt events, such as those discussed in this paper, appear to be related to a particular situation in which a large cyclonic storm system located off the Antarctic coast causes rapid transport of sea-salt-laden air to the vicinity of the Pole, appearing as a warming in the mid-troposphere. Surface warming and a weakening of the surface temperature inversion allow vertical transport for detection at the surface.

5. Acknowledgments

This work was performed as part of the ongoing NOAA/GMCC monitoring program. We thank J. Winchester of Florida State University for helpful discussions concerning the PIXE analysis, A. Hogan of the State University of New York at Albany for providing South Pole radiosonde data, and G. Walters of the National Center for Atmospheric Research, for providing the 500-mb height charts over the Antarctic continent.

REFERENCES

Ahlquist, N. C. and Charlson, R. J. 1969. Measurement of the wavelength dependence of atmospheric extinction due to scatter. *Atmos. Environ. 3*, 551–564.

Bodhaine, B. A. 1979. Measurement of the Rayleigh scattering properties of some gases with a nephelometer. *Appl. Opt. 18*, 121–125.

Bodhaine, B. A. 1983. Aerosol measurements at four background sites. *J. Geophys. Res. 88*, 10753–10768.

Bodhaine, B. A. and Bortniak, J. C. 1981. Four wavelength nephelometer measurements at South Pole. *Geophys. Res. Lett. 8*, 539–542.

Bodhaine, B. A. and Murphy, M. E. 1980. Calibration of an automatic condensation nuclei counter at the South Pole. *J. Aerosol Sci. 11*, 305–312.

Cunningham, W. C. and Zoller, W. H. 1981. The chemical composition of remote area aerosols. *J. Aerosol Sci. 12*, 367–384.

Cunningham, W. C., Etz, E. S. and Zoller, W. H. 1979. Raman microprobe characterization of South Pole aerosol. In: *Microbeam analysis*, ed. D. E. Newbury. San Francisco: San Francisco Press, 148–154.

Dennis, R. (ed.) 1976. *Handbook on aerosols*. TID-26608, National Technical Information Service, Springfield, Virginia, 142 pp.

Duce, R. A. 1972. Trace substances in the Antarctic atmosphere. *Proceedings of the Colloquium on Conservation Problems of Antarctica and Circumpolar Waters*, ed. B. Parker. Allen Press, Lawrence, Kansas, 27–42.

Duce, R. A., Zoller, W. H. and Jones, A. G. 1971. Atmospheric particle and gas sampling at McMurdo and South Pole stations. *Ant. J. United States 6*, 133–134.

Duce, R. A., Zoller, W. H. and Moyers, J. L. 1973. Particulate and gaseous halogens in the Antarctic atmosphere. *J. Geophys. Res. 78*, 7802–7811.

Duce, R. A., Hoffman, G. L. and Zoller, W. H. 1975. Atmospheric trace metals at remote northern and southern hemisphere sites: Pollution or natural? *Science 187*, 59–61.

Fischer, W. H., Lodge, J. P., Pate, J. B. and Cadle, R. D. 1969. Antarctic atmospheric chemistry: Preliminary exploration. *Science 164*, 66–67.

Harris, J. M. and Bodhaine, B. A. (eds.) 1983. *Geophysical monitoring for climatic change no. 11: summary report, 1982.* NOAA Air Resources Laboratory, Boulder, Colorado, 67–75.

Hofmann, D. J. and Rosen, J. M. 1985. Antarctic observations of stratospheric aerosol and high altitude condensation nuclei following the El Chichon eruption. *Geophys. Res. Lett. 12*, 13–16.

Hogan, A. W. 1975. Antarctic aerosols. *J. Appl. Meteorol. 14*, 550–559.

Hogan, A. W. 1979. Meteorological transport of particulate material to the south polar plateau. *J. Appl. Meteorol. 18*, 741–749.

Hogan, A. W. and Barnard, S. 1978. Seasonal and frontal variation in Antarctic aerosol concentrations. *J. Appl. Meteorol. 17*, 1458–1465.

Hogan, A. W., Barnard, S. and Bortniak, J. 1979. Physical properties of the aerosol at the South Pole. *Geophys. Res. Lett. 6*, 845–848.

Hogan, A. Barnard, S., Samson, J. and Winters, W. 1982. The transport of heat, water vapor and particulate material to the south polar plateau. *J. Geophys. Res. 87*, 4287–4292.

Ito, T. 1985. Study of background aerosols in the Antarctic Troposphere. *J. Atmos. Chem. 3*, 69–91.

Johansson, T. B., Van Grieken, R. E., Nelson, J. W. and Winchester, J. W. 1975. Elemental trace analysis of small samples by proton induced X-ray emission. *Anal. Chem. 47*, 855–859.

Komhyr, W. D. 1983. An aerosol and gas sampling apparatus for remote observatory use. *J. Geophys. Res. 88*, 3913–3918.

Maenhaut, W. and Zoller, W. H. 1977. Determination of the chemical composition of the South Pole aerosol by instrumental neutron activation analysis. *J. Radioanalyt. Chem. 37*, 637–650.

Maenhaut, W., Zoller, W. H., Duce, R. A. and Hoffman, G. L. 1979. Concentration and size distribution of particulate trace elements in the south polar atmosphere. *J. Geophys. Res. 84*, 2421–2431.

Metnieks, A. L. and Pollak, L. W. 1959. Instruction for use of photo-electric condensation nucleus counters. *Geophys. Bull. No. 16*, School of Cosmic Physics, Dublin Institute for Advanced Study, Dublin, Ireland.

Miller, S. W. and Bodhaine, B. A. 1982. Supersaturation and expansion ratios in condensation nuclei counters: An historical perspective. *J. Aerosol Sci. 13*, 481–490.

Murphy, M. E. and Bodhaine, B. A. 1980. The South Pole automatic condensation nuclei counter: instrument details and 5 years of observations. *NOAA Tech. Memo. ERL ARL-82*, NOAA Air Resources Laboratories, Silver Spring, Maryland, 88 pp.

Parungo, F., Ackerman, E., Caldwell, W. and Weickmann, H. K. 1979. Individual particle analysis of Antarctic aerosols. *Tellus 31*, 521–529.

Parungo, F., Bodhaine, B. and Bortniak, J. 1981. Seasonal variation in Antarctic aerosol. *J. Aerosol Sci. 12*, 491–504.

Skala, G. F. 1963. A new instrument for the continuous measurement of condensation nuclei. *Anal. Chem. 35*, 702–706.

Thielke, J. F., Charlson, R. J., Winter, J. W., Ahlquist, N. C., Whitby, K. T., Husar, R. B. and Liu, B. Y. H. 1972. Multiwavelength nephelometer measurements in Los Angeles smog aerosols II. Correlation with size distributions, volume concentrations. *J. Colloid Inter. Sci. 39*, 252–259.

van de Hulst, H. C. 1957. *Light scattering by small particles.* New York: Wiley, 470 pp.

Zoller, W. H., Gladney, E. S. and Duce, R. A. 1974. Atmospheric concentrations and sources of trace metals at the South Pole. *Science 183*, 198–200.